CrystEngComm

Cite this: *CrystEngComm*, 2012, **14**, 8076–8082

www.rsc.org/crystengcomm

PAPER

Synthesis and photoactivity enhancement of $ZnWO_4$ photocatalysts doped with chlorine†

Guangli Huang[ab] and Yongfa Zhu*[a]

Received 23rd June 2012, Accepted 22nd August 2012
DOI: 10.1039/c2ce26005k

$ZnWO_4$ photocatalysts doped with chlorine were synthesized by a simple hydrothermal process. The influences of chlorine doping on the crystal structure, optical properties and photocatalytic activities of the $ZnWO_4$ photocatalyst were investigated. $ZnWO_4$ doped with chlorine showed enhanced photocatalytic activity for the degradation of methylene blue (MB), rhodamine B and 4-chlorophenol. The photocatalytic activity of $ZnWO_4$ with $R_{Cl} = 0.3$ can be enhanced approximately 4 times for the degradation of MB. The enhanced photocatalytic activity originated from the increase of the transfer rate of photogenerated electrons to the photocatalyst surface, which was promoted by chlorine doping. The photodegradation process of MB can be described as N-demethylation and oxidative degradation. In the case of chlorine doping, an effective separation of the photogenerated electron–hole pairs and the fast interfacial charge transfer to the electron donor/electron acceptor occurred.

1. Introduction

Semiconductor photocatalytic processes have been widely applied as techniques for the destruction of organic pollutants in wastewater because of the advantages of photocatalytic degradation.[1] Recently, some reports revealed that $ZnWO_4$ showed high photocatalytic activity for the mineralization of organic pollutants under UV irradiation.[2–5] Its unique combination of physical and chemical properties, in terms of chemical inertness, photostability and environmentally friendly features, make us believe it is a good photocatalytic candidate material.[3] Therefore, improving the photocatalytic activity of $ZnWO_4$ for practical applications is significant and meaningful. In previous reports,[6,7] the introduction of fluorine enhanced the photocatalytic activity of $ZnWO_4$. However, one problem is still not resolved: the enhanced photocatalytic activity of F-doped $ZnWO_4$ is also not enough to meet the requirements of practical application.[8]

In the past few decades, among these improved investigations, the doping of chlorine has been proven as an effective method.[9–11] For example, TiO_2 co-doped with Cl and Br displayed an enhanced photocatalytic activity.[9] Chen *et al.*[10] prepared chlorine doped TiO_2 with a visible light response and the enhanced photocatalytic activity originated from a mixture of anatase–rutile. Xu *et al.*[11] found that chlorine doping can result in high photocatalytic activities because of higher surface acidity as well as crystal defects in the TiO_2 photocatalyst. Therefore, our group has tried to research the optical properties and photocatalytic activities of $ZnWO_4$ doped with chlorine.

Up to now, there are no reports on photocatalytic activity of $ZnWO_4$ doped with chlorine, although the luminescent properties of $ZnWO_4$ can be improved by chlorine doping.[13] In this work, $ZnWO_4$ doped with chlorine photocatalysts with different chlorine concentrations were synthesized by a hydrothermal process. Our principal aim is to understand the effects of chlorine introduction on the chemical properties of $ZnWO_4$. Methylene blue (MB) was chosen as a probe molecule to investigate the role of chlorine on the photocatalytic activity of the $ZnWO_4$ catalyst.

2. Experimental section

2.1 Synthesis of ZnWO4 doped with chlorine

$ZnWO_4$ samples doped with chlorine were prepared through a hydrothermal process. All the chemicals used were analytic grade reagents without further purification. $Zn(NO_3)_2{\cdot}6H_2O$ and $Na_2WO_4{\cdot}2H_2O$ (1 : 1 molar ratio) were mixed together and 100 mL of distilled water was added. White precipitates appeared immediately and the beaker was put in an ultrasonic bath for 30 min in order to complete the precipitated reaction. The precipitates were filtered off, washed several times with distilled water and then added to stainless steel autoclaves with a Teflon liner containing a mixed solution of 30 mL of distilled water and the desired amounts of NH_4Cl. In what follows, the value of R_{Cl} is used to describe the atomic ratio of Cl to Zn and represents 0, 0.1, 0.2, 0.3, 0.4 and 0.8 nominal atomic ratios in the synthesis solution. After being sealed, the autoclaves were heated in a

[a]*Department of chemistry, Tsinghua University, Beijing 100084, P. R China. E-mail: zhuyf@tsinghua.edu.cn; Fax: +86-10-62787601; Tel: +86-10-62783586*
[b]*Beijing Tobacco Quality Supervision and Test Station, Beijing 100029, P. R. China*
† Electronic supplementary information (ESI) available. See DOI: 10.1039/c2ce26005k

convection oven at 180 °C for 24 h. The products were collected by filtration and washed with distilled water several times until no Cl^- were left in the solution when tested. The samples were then dried at 80 °C for 4 h before characterization.

2.2 Characterization

The products were characterized by powder X-ray diffraction (XRD) on a Bruker D8-advance X-ray diffractometer at 40 kV and 40 mA with monochromatized Cu–Kα (λ = 1.5418 Å) radiation. The morphologies of the prepared samples were further examined with transmission electron microscopy (TEM) by a JEM 1200 electron microscope operated at an accelerating voltage of 100 kV. The Brunauer–Emmett–Teller (BET) surface area was determined by an ASAP 2010 V5.02H. The adsorbed gas was nitrogen. The X-ray photoelectron spectroscopy (XPS) analysis was measured on a PHI 5300 ESCA instrument using an Al–Kα X-ray source at a power of 250 W. Infrared transmission spectra were recorded with KBr disks containing the powder sample on an FT-IR spectrometer (Perkin-Elmer 1600). UV-Vis diffuse reflectance spectra (DRS) of the samples were measured using a Hitachi U-3010 UV-Vis spectrophotometer.

2.3 Photoelectrochemical measurement

As-prepared samples for the fabrication of the photoanode were obtained by mixing 1 mL of ethanol and 20 mg of the as-prepared powder homogeneously. The as-prepared samples were spread on an indium-tin oxide (ITO) conducting glass (3 cm × 2 cm) with a sheet resistance of 15 Ω. After the films were dried under ambient conditions, they were sintered in air at 400 °C for 1 h. Photoelectrochemical measurements were carried out in a conventional three electrode system. The as-prepared thin film with an ITO substrate and epoxy resin to prevent any current leakage served as the working electrode. A Pt wire and saturated calomel (SCE) were employed as the counter and reference electrodes, respectively. A quartz electrolytic cell was employed, filled with a 0.1 M Na_2SO_4 solution. The reactor (50 mm × 50 mm × 140 mm) was placed 3 cm away from a 15 W germicidal lamp (~90% of the energy output at 254 nm). The intensity of the light, as measured by a UV-irradiance meter (Instruments of Beijing Normal University), was 1 mW cm^{-2} at the position where the film electrode was placed. Electrochemical impedance spectra (EIS) were carried out with a computerized CHI660B electro-chemical system (Shanghai, China). They were recorded in the potentiostatic mode. The amplitude of the sinusoidal wave was 10 mV and the frequency range of the sinusoidal wave was from 100 kHz to 0.05 Hz. Mott-Schottky spectra were obtained with a PARSTAT-2273 Advanced Electrochemical System (Princeton Applied Research) equipped with an impedance analyzer and controlled by a computer.

2.4 Photocatalytic test

The photoactivities of the samples were evaluated by the degradation of methylene blue (MB) and rhodamine B (RhB) under ultraviolet light irradiation of 11 W from a low pressure lamp at 254 nm. The average light intensity was 1.0 mW cm^{-2}. The radiant flux was measured with a power meter from the Institute of Electric Light Source (Beijing). RhB and MB solutions (200 mL, 1.0 × 10^{-5} molL^{-1}) containing 0.10 g of the as-prepared samples were put into a glass beaker. Before the light was turned on, the solution was first ultrasonicated for 10 min and then stirred for 30 min to ensure equilibrium between the catalysts. 3 mL of the sample solutions was taken at given time intervals and separated through centrifugation (4,000 rpm, 10 min). The supernatants were analyzed by recording variations in the absorption band maximum (553 nm for RhB and 663 nm for MB) using a U-3010 spectrophotometer (Hitachi). All the experiments were carried out at least twice. The reported values are within the experimental error of ±3%.

3. Results and discussion

3.1 Photocatalytic activity enhancement by chlorine doping

The photocatalytic activity of the as-prepared samples was first evaluated through the degradation of MB in aqueous solution. Fig. 1a shows the photocatalytic degradation curve of MB as a function of time. The first-order linear relationship was revealed

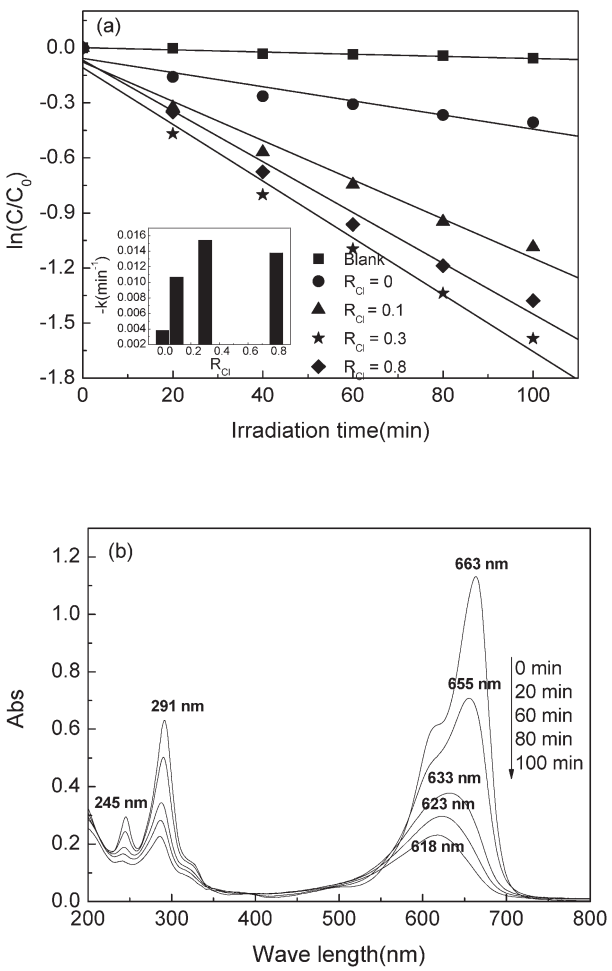

Fig. 1 (a) The photocatalytic activity of the various samples with different doped chlorine concentrations and the dependence of the apparent rate constants (k/min^{-1}) and Cl amount (inset). Catalyst loading, 0.50 g L^{-1}; MB, 1.0 × 10^{-5} mol L^{-1}; (b) The temporal evolution of the spectral changes during the photodegradation of MB over $ZnWO_4$ with R_{Cl} = 0.3 and the structure of the MB molecule (inset).

by plots of $\ln(C/C_0)$ *vs.* the irradiation time. The blank test confirms that the photolysis of MB can be ignored. The chlorine doped samples exhibit higher photocatalytic activities than that of un-doped $ZnWO_4$. The influence of chlorine doped amounts upon the photodegradtion rate of MB is also shown (Fig. 1a, inset). The apparent reaction constant k is 0.38×10^{-2}, 1.07×10^{-2}, 1.54×10^{-2}, 1.38×10^{-2} min^{-1}, respectively, for the chlorine doped ratios of R_{Cl} of 0, 0.1, 0.3 and 0.8. The photocatalytic activity of the samples increases with an increasing chlorine dopant concentration. The sample with R_{Cl} = 0.3 shows the highest activity, which is 4 times higher than that of un-doped $ZnWO_4$. However, on further increasing of the chlorine dopant concentration, the photocatalytic activity of the as-prepared samples decreases. The optimal doped amount of chlorine is 0.3.

The photocatalytic activities of the as-prepared samples were also evaluated by through the degradation of RhB in aqueous solution (in Fig. S1, ESI†). The sample with R_{Cl} = 0.3 shows the highest activity and the k value reaches the highest value of 4.34×10^{-2} min^{-1}, which is 2.5 times compared with that of un-doped $ZnWO_4$. The 4-chlorophenol photodegradation with the as-prepared samples displays similar results (Fig. S2, ESI†). Based on the above results, it can be found that the chlorine doped $ZnWO_4$ photocatalyst shows a high activity for degradation of organic contaminants. This result implies that chlorine doping plays an important role in the enhancement of the photocatalytic activity.

Fig. 1b presents the temporal evolution of the spectral changes during the photodegradation of MB over $ZnWO_4$ with R_{Cl} = 0.3 at various time intervals. It can be found that the absorbance peaks at 246, 291 and 663 nm, which are all associated with MB, decrease on increasing the irradiation time but the absorbance band at 256 nm (contributed by leuco-MB) does not appear at all. This indicates that the MB discoloration observed in this study should be due to oxidative degradation.[14] It also shows that the band at 663 nm blue shifts by as much as 45 nm from 663 nm to 618 nm during the photodegradation process. This illustrates that MB degradation occurs *via* N-demethylation.[15] After methyl or methylamine in the MB structure is degraded, the color of MB becomes less intense.[16] Therefore, N-demethylation and oxidative degradation occurs during the photodegradation process of MB.

Chlorine doped $ZnWO_4$ with R_{Cl} = 0.3 as a type of heterogeneous photocatalyst can be easily recycled by a simple filtration because of its large density. After three cycles of the photodegradation of RhB, the catalyst did not exhibit any significant loss of activity, as shown in Fig. 2, confirming that the as-prepared catalyst is not photocorroded during the photocatalytic oxidation of the pollutant molecules. XRD analysis of the sample (in Fig. S3, ESI†) also shows that the crystal structure of the photocatalyst is not changed after the photocatalytic reaction, indicating that the sample is fairly stable during the photodegradation process.

3.2 Effect of chlorine doping on the structure of $ZnWO_4$ photocatalyst

Fig. 3a shows the XRD patterns of the samples with different doped chlorine concentrations. All of the as-prepared samples

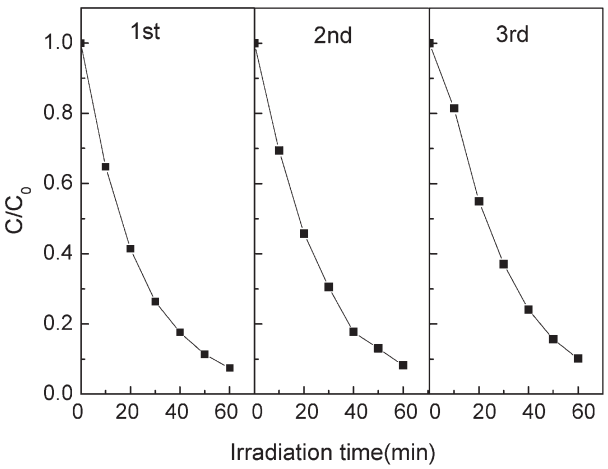

Fig. 2 Cycling runs in the photocatalytic degradation of RhB in the presence of chlorine doped $ZnWO_4$ with R_{Cl} = 0.3; catalyst loading: 0.5 g L^{-1}; initial concentration of RhB, 1×10^{-5} M.

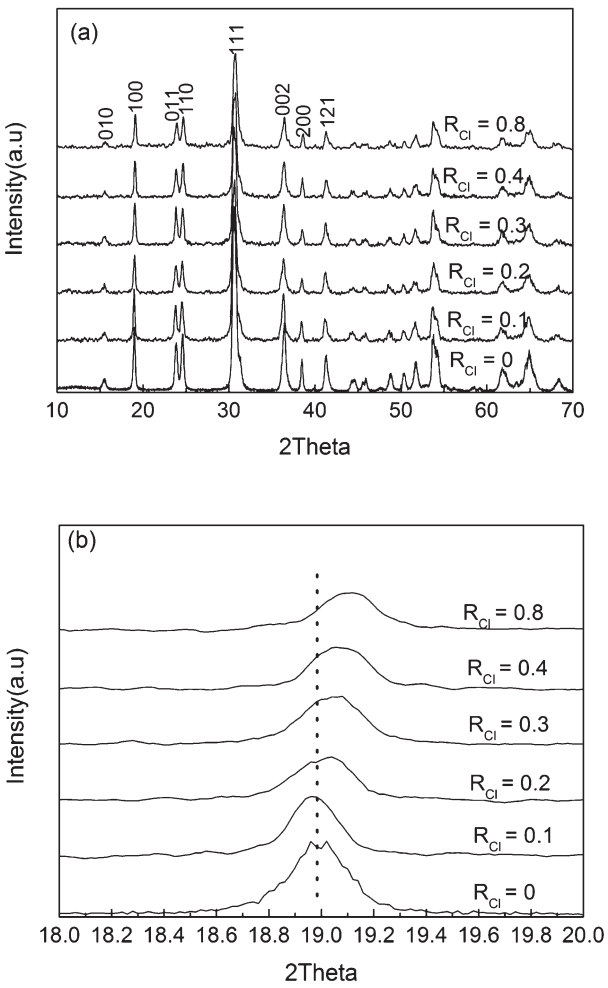

Fig. 3 (a) XRD patterns of the samples with different R_{Cl} values; (b) Diffraction peak positions of the (100) plane in the range of 2θ = 18–20°

appear to be phase-pure $ZnWO_4$, which demonstrates that chlorine doping does not result in the development of new crystal orientations or change the preferential orientations. Further observation shows that the peak intensities of $ZnWO_4$ become weaker on increasing the R_{Cl} ration and the diffraction peaks of $ZnWO_4$ are wider, indicating the reduction in crystallization and the formation of smaller $ZnWO_4$ crystallites. The presence of chlorine ions could play an important role in the formation of $ZnWO_4$ crystals. Chlorine ions were involved in the process of the crystallization, resulting in more vacancies in the $ZnWO_4$ crystal, which is in good agreement with the XRD results of fluorinated Bi_2WO_6.[17]

However, further observation of the (100) diffraction peaks in the range of 2θ = 18–20° (Fig. 3b) shows that the peak position of chlorine doped $ZnWO_4$ shifts slightly towards a higher 2θ value with an increase in the chlorine concentrations. The other diffraction peaks present the same results. These changes may be caused by chlorine doping. It is known that many factors, such as the differences between the ionic radius and the electronegativity, can induce changes in the lattice parameters.[11] Because significant differences exist between the ionic radius of Cl^- (0.180 nm) and O^{2-} (0.144 nm), the cell parameters change with the increase of the Cl concentration. When there are certain gradients along the concentration distribution of the dopant chlorine in $ZnWO_4$, the oxygen ions cannot match well with the concentration gradients of chlorine. This would result in a large lattice distortion. In addition, more room is needed when Cl doping of $ZnWO_4$ occurs because the size of the Cl^- ion and O^{2-} ion is in the order of O < Cl.[12] Based on this, the observed shift of the diffraction peak towards a higher angle indicates that chlorine doping into $ZnWO_4$ occurred.

An XPS survey spectrum of the chlorine doped $ZnWO_4$ catalyst with R_{Cl} = 0.4 (nominal atomic ratio) is shown in Fig. 4. It demonstrates that the chlorine doped $ZnWO_4$ samples are composed of Zn, W, O, Cl and a trace amounts of carbon. Quantitative analysis demonstrates that the surface atomic ratio of Cl/Zn is 0.04 and 0.06, when R_{Cl} = 0.1 and R_{Cl} = 0.4, respectively. An XPS spectrum of the Cl 2p peak is shown in the inset of Fig. 4. The intensity of the Cl 2p peak increases when the doped chlorine concentration increases. The binding energy of the Cl 2p orbital is 199.2 eV. Generally, a Cl 2p binding energy of 198.3 eV corresponds to the chlorine absorbed onto TiO_2 and a value of 198.0 eV corresponds to chlorine within the lattice.[18] However, according to the results for K_2WCl_6[19] and the XRD, the chlorine ions are in the lattice of $ZnWO_4$. The XPS survey spectra of the other as-prepared samples are similar. Therefore, it can be inferred that the contribution of the Cl 2p peak is from chlorine ions in the lattice of the $ZnWO_4$ crystal. This result is in agreement with the XRD results (in Fig. 3).

Fig. 5 shows the FT-IR spectra of the $ZnWO_4$ catalyst with different doped chlorine concentrations. In Fig. 5a, the broad band at 3300–3600 cm^{-1} and the peak at 1626 cm^{-1} are attributed to the stretching vibration and bending vibration of O–H,[5] and the peak at 1400 cm^{-1} corresponds to an OH absorption of hydrogen related defects. The intensity of the peak at 1400 cm^{-1} increases with an increase in the doped chlorine concentration, indicating the increasing number of defects in the crystals.[5] This result conforms to the XRD results, which shows

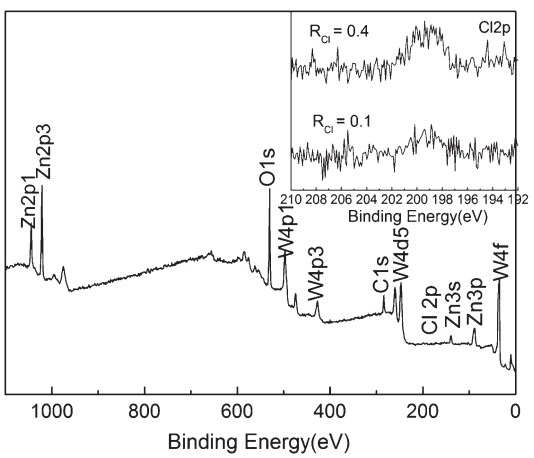

Fig. 4 XPS survey spectrum of chlorine doped $ZnWO_4$ with R_{Cl} = 0.4. The inset is the Cl 2p peak intensity of the as-prepared samples with R_{Cl} = 0.1 and R_{Cl} = 0.4.

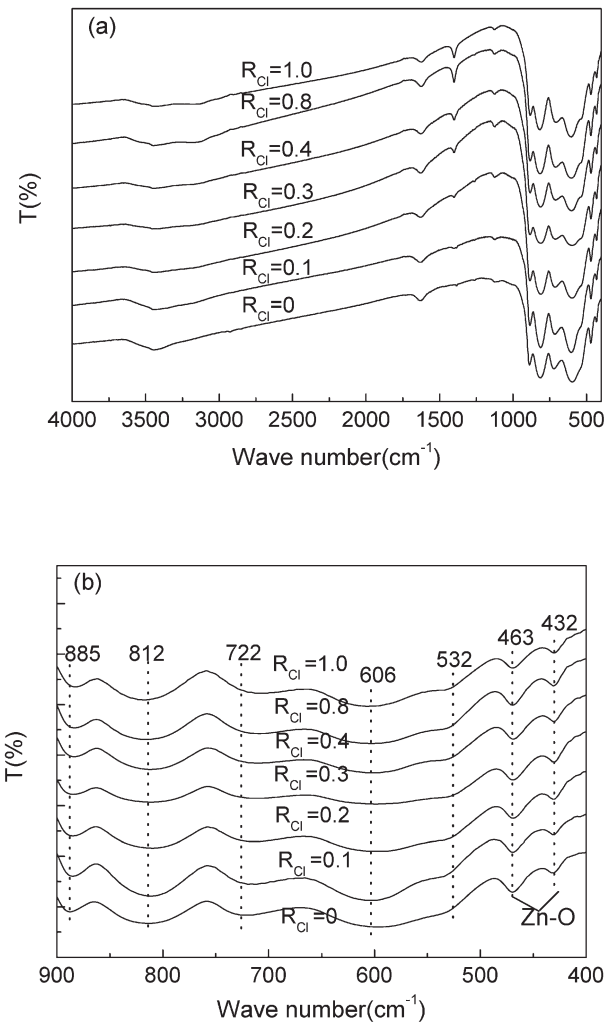

Fig. 5 (a) FT-IR spectra of the $ZnWO_4$ catalysts with different doped chlorine concentrations; (b) A careful comparison in the range of 900–400 cm^{-1}.

that chlorine doping resulted in the distortion of the crystal lattice.

The peaks in the range of 900–400 cm^{-1}, shown in Fig. 5b, are assigned to the stretching vibrations of $ZnWO_4$.[20,21] The bending and stretching vibrations of Zn–O occur at 463 and 432 cm^{-1}. The stretching and bending vibrations of W–O occur at 885, 812, 722, 606 and 532 cm^{-1}. Further observation of the peaks in the 900–400 cm^{-1} region shows that the shape and location of the peaks are unchanged on increasing the doped chlorine concentration but the peak at 722 cm^{-1} shifts to 703 cm^{-1} in the R_{Cl} range from 0 to 1.0 and the bands at 606 cm^{-1} shift to a higher wave number. A comparison with the IR results of fluorine doped $ZnWO_4$[6] indicates that the effect of chlorine doping on WO_6 is smaller than that of fluorine doping. This may be attributed to the ionic radius and electronegativity as the doping of chlorine is more difficult than that of fluorine.

TEM photographs of the as-prepared samples are shown in Fig. 6. The morphologies of the samples are homogeneous. In the R_{Cl} range from 0 to 1.0, the particle sizes in the samples are the same and on the scale of 30–50 nm. When the value of R_{Cl} is 0, 0.1, 0.2, 0.3, 0.4 and 0.8, the specific surface area is 20.0, 24.9, 23.6, 23.3, 23.3 and 20.1 $m^2\ g^{-1}$, respectively.

3.3 Effect of chlorine doping on the photoelectric properties

The UV-visible diffuse reflectance spectra of the chlorine doped samples are shown in Fig. 7. They show that the samples with different amounts of chlorine present almost the same absorption edges. The band gaps of the samples with $R_{Cl} = 0$ and $R_{Cl} = 0.4$ are estimated to be 3.70 eV and 3.68 eV, respectively (Fig. 7, inset). The absorption of $ZnWO_4$ in the UV region was assigned to the band transition from the occupied O 2p orbital to the empty W 5d orbital.[22] Furthermore, it can be found that the shape did not change after chlorine doping but chlorine doping obviously affects the intensity of the light absorption. The chlorine doped $ZnWO_4$ samples show a stronger absorption in the UV-visible range. Generally, the rate of the photocatalytic

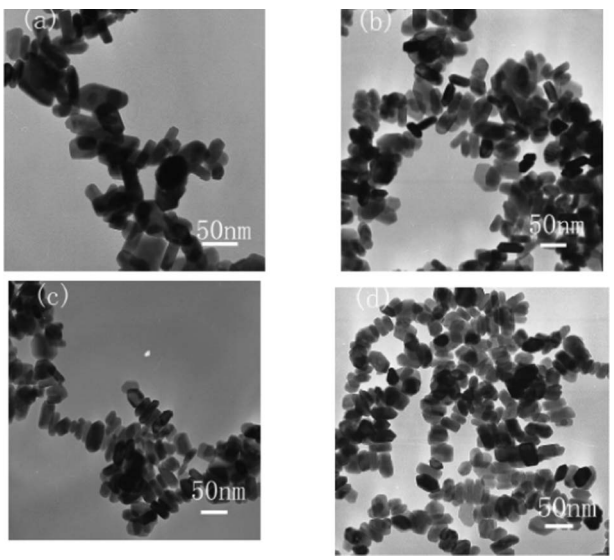

Fig. 6 TEM photographs of the $ZnWO_4$ samples with different Cl amounts. (a) $R_{Cl} = 0$; (b) $R_{Cl} = 0.3$; (c) $R_{Cl} = 0.4$; (d) $R_{Cl} = 0.8$

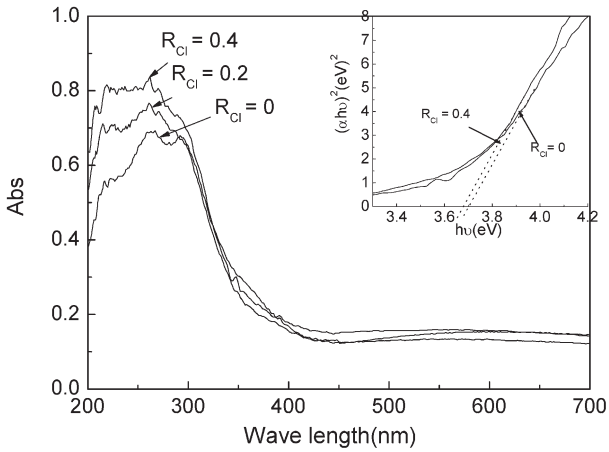

Fig. 7 UV-visible diffuse reflectance spectra of the $ZnWO_4$ samples with different doped chlorine concentrations.

reaction is proportional to $(I_\alpha \Phi)^n$ (n = 1 for low light intensity and n = 1/2 for high light intensity), where I_α is the photo numbers adsorbed by the photocatalyst per second and Φ is the efficiency of the band gap transition. Therefore, an increase in α (absorption coefficient) or $I_\alpha \Phi$, resulting from the intensive absorbtion, can result in the enhancement of the photocatalytic activity of chlorine doped $ZnWO_4$.[23]

The transport of photogenerated electrons through the n-type semiconductor to the collecting electrode is believed to occur by diffusion within the extended states, slowed by trapping/detrapping events.[24] To understand the difference in the electronic properties of the $ZnWO_4$-based electrodes, Mott-Schottky (MS) measurements (Fig. 8a) were performed in the dark using the impedance technique.[25] A reversed sigmoidal plot was observed with an overall shape that is consistent with typical n-type semiconductors.[26]

As is known from the classical Mott-Schottky theory, when the doping semiconductor space-charge region is depleted, as it is under biasing conditions, the capacitance of the space-charge region can be described after simplification as:

$$\frac{1}{C^2} = \left(\frac{2}{eN_d\varepsilon_0\varepsilon}\right)\left|V - V_{fb} - \frac{kT}{e}\right| \quad (1)$$

where e is the electronic charge (1.6×10^{-19} C), ε_0 is the permittivity of free space (8.86×10^{-12} F m^{-1}), ε is the dielectric constant (16.6 F m^{-1}) of the $ZnWO_4$ material, N_d is the dopant (donor or acceptor) concentration, k is the Boltzmann constant (1.38×10^{-23} J K^{-1}), T is the absolute temperature, V is the applied potential and V_{fb} is the flat-band potential.[27] It shows that when $1/C^2$ is zero, the x-intercept is equal to the flat-band potential V_{fb}, and the dopant density N_d can be determined from the slope of the linear region.

Based on Fig. 8a, the V_{fb} potential of the as-prepared samples are obtained. The calculated V_{fb} value for $ZnWO_4$ electrodes with R_{Cl} = 0, 0.1, 0.3, 0.4 and 0.8 is −0.40, −0.38, −0.50, −0.42 and −0.45 V *vs.* Ag/AgCl (in saturated KCl), respectively. The V_{fb} value of $ZnWO_4$ films with a pH 6.0 electrolyte was reported to be approximately −0.36 V *vs.* SCE.[28] Almost agreeable results are obtained in this research system. The V_{fb} value of the doped $ZnWO_4$ shows a negative shift of the conduction band when

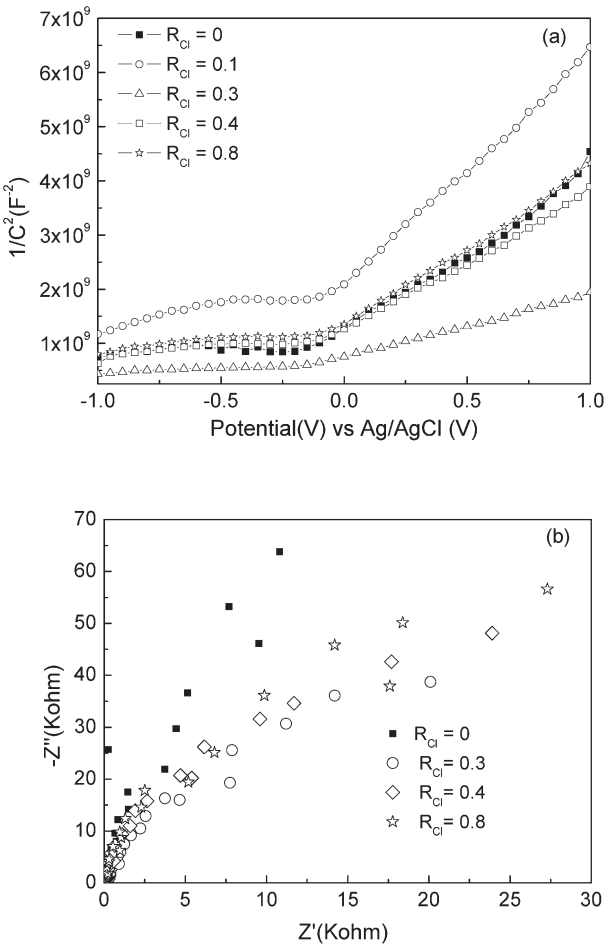

Fig. 8 Electrochemical properties of the different catalyst film electrodes. (a) Mott-Schottky (MS) plots obtained at a frequency of 1 kHz; (b) EIS Nynquist plots obtained under UV light.

compared with the un-doped $ZnWO_4$, except for the sample with $R_{Cl} = 0$.

In some cases, the presence of a large number of surface states or oxygen vacancies can result in a considerable change in the band position[29] In addition, the slope of the linear region for the doped sample shows a much lower value, clearly indicating a significantly higher donor density for the doped electrode. According to the photocatalytic mechanism,[29] the higher the donor density for the doped electrode, the faster the photocatalytic degradation rate.

To investigate the influence of chlorine doping on the photoelectric property, EIS technology was used to study the solid/electrolyte interfaces of the $ZnWO_4$ and Cl-doped $ZnWO_4$ sample under UV light irradiation (Fig. 8b). According to conventional double-layer theories, the electrical double layer at the solid electrode behaved as a frequency distribution impedance instead of a pure capacitance due to the surface heterogeneity. When the charge transfer reaction occurred, the Nyquist plot was a semicircle. When the semi-infinite diffusion was the rate-determining step, a linear plot with a slope of 45° appeared.[30,31] In our case, the arc radius on the EIS Nynquist plots of the chlorine doped film samples are smaller than that of the undoped film sample, which is evidence that an effective separation of the photogenerated electron–hole pairs and fast interfacial charge transfer to the electron donor/electron acceptor occurred as suggested.[32] Thus, in the case of chlorine doped $ZnWO_4$, the photoinduced electron–hole pairs are more easily separated and transferred to the sample surface. This result also supports the MS conclusion.

3.4 Effect of chlorine doping on the mechanism of high photoactivities

The photocatalytic activity was governed by various factors, such as surface area, phase structure, particle size, interfacial charge transfer and separation efficiency of the photoinduced electrons and holes.[33] In this work, the as-prepared samples have similar phase structures and almost the same particle sizes. The specific surface area of chlorine doped $ZnWO_4$ changes little. Therefore, it can be inferred that the phase structure, particle size and specific surface area play minor roles in enhancing the photocatalytic activity in this work. There are other factors that affect the photocatalytic activities of the as-prepared samples.

It is known that the photocatalytic activities of semiconductor materials are controlled by the ratio of the surface electrons transfer rate to the electron–hole recombination rate. If the surface electrons transfer rate occurs too quickly or the electron–hole recombination rate is slow, this favors the occurance of a chemical reaction.[23] Based on the results above (Fig. 8), the order of the arc radius on the EIS Nynquist plot of the chlorine doped film samples is consistent with the order of their photocatalytic activities, showing that an effective separation of the photogenerated electron–hole pairs is positively relevant to the photocatalytic activities. Furthermore, the increase in the intensive absorbance (Fig. 7) resulted in an increase in the rate of photogenerated electrons to the surface, leading to an effective participation in the surface reaction.[23] Therefore, the chlorine doped samples exhibited higher photoactivity than the un-doped samples. This conclusion has also been proved by previous reports.[10,11] However, when the dopant concentration becomes too high ($R_{Cl} > 0.3$), the recombination rate will increase because the distance between the trapping sites in a particle decreases with the number of dopant ions.

4. Conclusions

Chlorine doped $ZnWO_4$ has been synthesized. The photocatalytic activity can be enhanced 4 times for the direct photocatalytic degradation of MB. The doped photocatalyst is a promising photocatalytic material with a higher efficiency, which has good potential applications in environmental purification.

Acknowledgements

This work was partly supported by the National Natural Science Foundation of China (20925725 and 50972070) and 863 program (2012AA062701) and Tsinghua University Initiative Scientific Research Program.

References

1 M. R. Hoffmann, S. T. Martin, W. Choi and D. W. Bahnemann, *Chem. Rev.*, 1995, **95**, 69–96.
2 X. Zhao and Y. F. Zhu, *Environ. Sci. Technol.*, 2006, **40**, 3367–3372.

3 H. B. Fu, J. Lin, L. W. Zhang and Y. F. Zhu, *Appl. Catal., A*, 2006, **306**, 58–67.
4 G. L. Huang, C. Zhang and Y. F. Zhu, *J. Alloys Compd.*, 2007, **432**, 269–276.
5 R. Shi, Y. J. Wang, D. Li, J. Xu and Y. F. Zhu, *Appl. Catal., B*, 2010, **100**, 173–178.
6 G. L. Huang and Y. F. Zhu, *J. Phys. Chem. C*, 2007, **111**, 11952–11958.
7 L. W. Zhang and Y. F. Zhu, *Catal. Sci. Technol.*, 2012, **2**, 694–706.
8 H. G. Sun, W. L. Fan, Y. L. Li, X. F. Cheng, P. Li and X. Zhao, *J. Solid State Chem.*, 2010, **183**, 3052–3057.
9 H. M. Luo, T. Takata, Y. Lee, J. F. Zhao, K. Domen and Y. S. Yan, *Chem. Mater.*, 2004, **16**, 846–849.
10 H. Chen, M. C. Long, J. Xu and W. M. Cai, *Chin. J. Catal.*, 2006, **27**, 890–894.
11 H. Xu, Z. Zheng, L. Z. Zhang, H. L. Zhang and F. Deng, *J. Solid State Chem.*, 2008, **181**, 2516–2522.
12 K. Yang, Y. Dai, B. B. Huang and M. H. Whangbo, *Chem. Mater.*, 2008, **20**, 6528–6534.
13 R. Dafinova, K. Papazova and A. Bojinova, *J. Mater. Sci. Lett.*, 1998, **17**, 237–239.
14 H. Park and W. Choi, *J. Phys. Chem. B*, 2005, **109**, 11667–11674.
15 T. Y. Zhang, T. Oyama, A. Aoshima, H. Hidaka, J. C. Zhao and N. Serpone, *J. Photochem. Photobiol., A*, 2001, **140**, 163–172.
16 T. Mohammad and H. Morrison, *Photochem. Photobiol.*, 2000, **71**, 369–381.
17 H. B. Fu, S. C. Zhang, T. G. Xu, Y. F. Zhu and J. M. Chen, *Environ. Sci. Technol.*, 2008, **42**, 2085–2091.
18 H. Yun, J. Li, H. B. Chen and C. J. Lin, *Electrochim. Acta*, 2007, **52**, 6679–6685.
19 G. J. Leigh and W. Bremser, *J. Chem. Soc., Dalton Trans.*, 1972, 1216–1219.
20 V. V. Formichev and O. L. Kondratov, *Spectrochim. Acta, Part A*, 1994, **50**, 1113–1120.
21 J. P. Lesne and P. Caillet, *Can. J. Spectrosc.*, 1973, **18**, 69.
22 V. Nagirnyi, M. Kirm, A. Kotlov, A. Lushchik and L. Jonsson, *J. Lumin.*, 2003, **102–103**, 597–603.
23 A. Hattori and H. Tada, *J. Sol-Gel Sci. Technol.*, 2001, **22**, 47–52.
24 A. Zaban, A. Meier and B. A. Gregg, *J. Phys. Chem. B*, 1997, **101**, 7985–7990.
25 K. Y. Tse, B. M. Nichols, W. S. Yang, J. E. Butler, J. N. Russell and R. J. Hamers, *J. Phys. Chem. B*, 2005, **109**, 8523–8532.
26 F. Fabregat-Santiago, G. Garcia-Belmonte, J. Bisquert, P. Bogdanoff and A. Zaban, *J. Electrochem. Soc.*, 2003, **150**, 293–298.
27 G. Wang, Q. Wang, W. Lu and J. Li, *J. Phys. Chem. B*, 2006, **110**, 22029–22034.
28 X. Zhao, W. Q. Yao, Y. Wu, S. C. Zhang, H. P. Yang and Y. F. Zhu, *J. Solid State Chem.*, 2006, **179**, 2562–2570.
29 H. Maeda, K. Ikeda, K. Hashimoto, K. Ajito, M. Morita and A. Fujishima, *J. Phys. Chem. B*, 1999, **103**, 3213–3217.
30 W. H. Leng, Z. Zhang, J. Q. Zhang and C. N. Cao, *J. Phys. Chem. B*, 2005, **109**, 15008–15023.
31 H. Liu, S. A. Cheng, M. Wu, H. J. Wu, J. Q. Zhang, W. Z. Li and C. N. Cao, *J. Phys. Chem. A*, 2000, **104**, 7016–7020.
32 L. W. Zhang, H. B. Fu and Y. F. Zhu, *Adv. Funct. Mater.*, 2008, **18**, 2180–2189.
33 A. L. Linsebigler, G. Lu and J. T. Yates, *Chem. Rev.*, 1995, **95**, 735–758.